Maritime Technology and Society
Vol. 5(2): 242-251, June 2026
doi.org/10.62012/mp.vi.47792

Regular Research Article

Numerical Modeling and Simulation of Tsunami Hazards in South Seram Island, Indonesia: A Case Study on Kairatu Fault

Teddy Dwi Riadi[1*], Simon Tubalawony[2], Yunita Angnetjie Noya[2], Verry Bambang Sakiran[3]

[*1]Postgraduate Student, Marine Science Study Program, Pattimura University Postgraduate, Indonesia
[2]Marine Science Study Program, Faculty of Fisheries and Marine Sciences, Pattimura University, Indonesia
[3]Engineering Profesional Program Study Program, Faculty of Engineering, Katolik Widya Mandala Surabaya University, Indonesia

[*]teddy.black.21@gmail.com

Abstract: This study aims to analyze the potential for tsunamis caused by tectonic activity along the Kairatu Fault and to evaluate inundation patterns based on numerical modeling results using the COMCOT software. The Kairatu Fault is an active structure in the western part of Seram, with the potential to generate significant earthquakes and trigger tsunamis around Piru Bay and the waters of Ambon. Modeling was conducted using bathymetry data, earthquake source parameters, and seafloor deformation derived from the Okada model. Tsunami simulations were performed to estimate the maximum wave height, wave arrival time, and wave energy distribution along the coastline. Simulation results indicate that the southern coastal areas of Seram and the western coast of Ambon are highly vulnerable to inundation, with wave heights reaching 2–3 m and arrival times around 15–25 min after the earthquake event. Based on these modeling results, it is recommended that the early warning system and coastal spatial planning be strengthened to support tsunami disaster mitigation efforts in the area.

Keywords: tsunami, inundation, Kairatu Fault, COMCOT, mitigation

1. Introduction

Indonesia is one of the most seismically active countries in the world because it is located at the convergence of the Indo-Australian, Eurasian, and Pacific tectonic plates. The interaction among these major tectonic systems generates frequent earthquakes and contributes significantly to tsunami hazards throughout the Indonesian archipelago [1], [2]. Historical records indicate that numerous destructive earthquakes and tsunamis have occurred in Indonesia, causing substantial impacts on coastal communities, infrastructure, and economic activities [3].

The Maluku region, particularly Seram Island and its surrounding waters, is characterized by a complex tectonic environment controlled by active fault systems and regional plate interactions. Several active structures have been identified in this area, including the Kairatu Fault, Kawa Fault, and North Seram Fault [4]. These faults can generate moderate-to-large earthquakes that may induce seabed deformation and subsequently trigger tsunami waves.

The Kairatu Fault is in the western part of Seram Island and extends approximately parallel to the coastline. Earthquake activity associated with this fault system has been observed repeatedly, indicating its role as an important source of regional seismic hazards [5]. Furthermore, the 2019 Ambon earthquake sequence demonstrated that tectonic activity in

Received: 2025-10-15; Accepted: 2026-03-31
doi.org/10.62012/mp.vi.47792 | e-ISSN: 2828-6669 p-ISSN: 2828-7010

the region remains significant and capable of generating damaging seismic events [6].

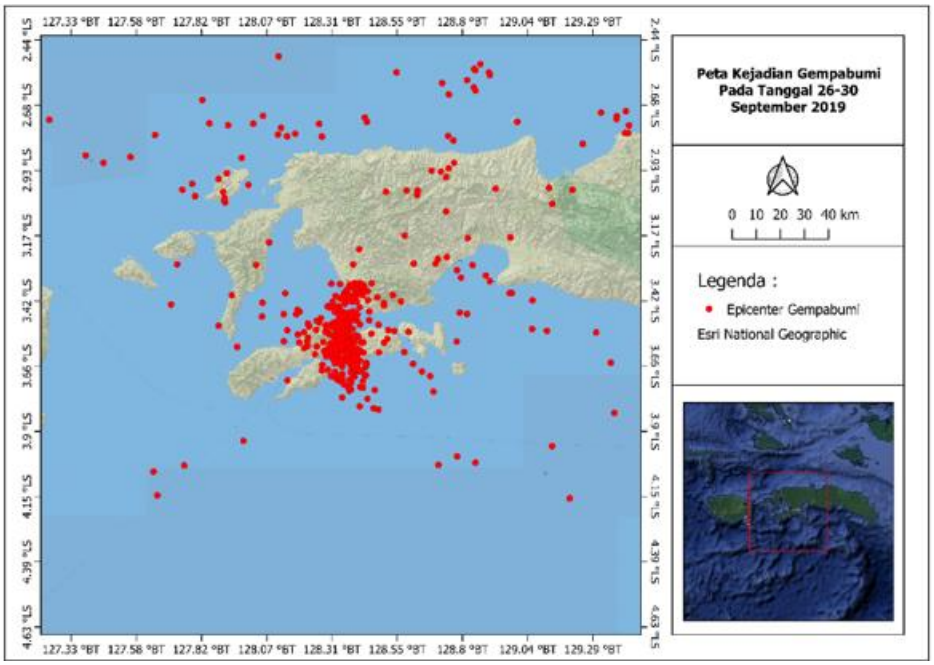

Figure 1. Historis Gempabumi Kairatu 2019

Figure 1 presents the historical earthquake distribution in the Kairatu Fault region based on data obtained from the Meteorology, Climatology, and Geophysics Agency (BMKG). The concentration of earthquake epicenters highlights the active tectonic nature of the study area and emphasizes the importance of evaluating potential tsunami impacts associated with future seismic events.

The identification of active faults is essential for assessing future earthquake and tsunami hazards because fault geometry, rupture dimensions, and source mechanisms strongly influence tsunami generation processes [7], [8]. Although previous studies have investigated regional tectonics and seismicity in eastern Indonesia, detailed assessments of tsunami generation and inundation associated with the Kairatu Fault remain limited. Consequently, uncertainties remain regarding potential tsunami heights, arrival times, and inundation extents along the surrounding coastlines.

Numerical tsunami modeling has become an effective approach for evaluating tsunami hazards and supporting disaster mitigation planning. The Cornell Multi-grid Coupled Tsunami Model (COMCOT) is widely applied for tsunami generation, propagation, and inundation simulations because of its ability to solve shallow-water equations efficiently using nested computational grids [9]. Therefore, this study aims to evaluate tsunami hazards generated by a hypothetical Mw 6.5 earthquake along the Kairatu Fault combined with submarine landslide scenarios. The analysis focuses on tsunami propagation characteristics, estimated arrival times, maximum wave heights, and potential inundation areas. The results are expected to support coastal disaster risk reduction and tsunami mitigation planning in South Seram Island and surrounding regions.

2. Material and Methode

2.1. Material

The input data required for tsunami modeling consisted of bathymetric data, topographic data, land cover data, landslide parameters, and earthquake parameters. The bathymetric data, topographic data, and land cover data used in this model were obtained from the National Bathymetry Data (BATNAS), National Digital Elevation Model (DEMNAS), and Indonesian Earth Surface Map (RBI), respectively, provided by the Indonesian Geospatial Information Agency (BIG) [10].

The landslide and earthquake parameters used in this study were assumed to be based on the analysis of potential earthquake and landslide sources in the eastern part of Ambon City. These parameters were incorporated into several source scenarios for tsunami generation.

Received: 2025-10-15; Accepted: 2026-03-31
doi.org/10.62012/mp.vi.47792 | e-ISSN: 2828-6669 p-ISSN: 2828-7010

All datasets were processed and converted into formats compatible with the tsunami modeling software [11], [12].

This study used secondary data obtained from relevant institutions and publicly available sources. The earthquake source was assumed to have a magnitude of 6.5, while the landslide source was assumed to have a volume of 0.10 km³ based on the observed bathymetric conditions. The earthquake and landslide input parameters used in the model are presented in Tables 1 and 2, respectively [13], [14], [15].

Table 1. Earthquake Input Data

Parameter	Value
Earthquake magnitude	6.5
Source location	Eastern part of Ambon City
Data type	Assumed scenario data
Number of source scenarios	3

Table 2. Landslide Input Data

Parameter	Point 1	Point 2
Volume (km³)	0.10	0.10
X start	128.3497655	128.4408771
X stop	128.3480922	128.4327945
Y start	-3.35696596	-3.45207299
Y stop	-3.37154739	-3.46401323
Slope (°)	30	30
Length (m)	650	600
Width (m)	770	835
Thickness (m)	200	200

2.2. Mathematical Model of Tsunami Wave Propagation

Tsunami waves are generally classified as long waves because their wavelengths are much greater than the local water depth. Under these conditions, vertical acceleration is negligible compared with gravitational acceleration, allowing the application of the shallow-water approximation [9], [10]. Consequently, tsunami propagation can be represented using continuity and momentum equations derived from the conservation of mass and momentum principles.

2.3. Continuity Equation

The continuity equation expresses the conservation of mass for incompressible fluids and can be written as:

$$\frac{\partial \eta}{\partial t} + \frac{\partial M}{\partial x} + \frac{\partial N}{\partial y} = 0 \qquad (1)$$

$$M = \int_{-h}^{\eta} u dz = \bar{u}(\eta + h) \qquad (2)$$

$$N = \int_{-h}^{\eta} v dz = \bar{v}\,(\eta + h) \qquad (3)$$

where M and N represent volume fluxes in the x and y directions (m²/s), respectively. The variables h and η denote water depth and free-surface elevation, while u and v represent depth-averaged flow velocities in the x and y directions.

2.4. Momentum Equation

The momentum equations describe the conservation of momentum in fluid motion and are formulated as:

$$\frac{\partial u}{\partial t} + u\frac{\partial u}{\partial x} + v\frac{\partial u}{\partial y} + w\frac{\partial u}{\partial z} = \frac{-1}{\rho}\frac{\partial \rho}{\partial x} - \frac{1}{\rho}\left(\frac{\partial \tau_{xx}}{\partial x} + \frac{\partial \tau_{xy}}{\partial y} + \frac{\partial \tau_{xz}}{\partial z}\right) \qquad (4)$$

$$\frac{\partial v}{\partial t} + u\frac{\partial v}{\partial x} + v\frac{\partial v}{\partial y} + w\frac{\partial v}{\partial z} = \frac{-1}{\rho}\frac{\partial \rho}{\partial y} - \frac{1}{\rho}\left(\frac{\partial \tau_{xx}}{\partial x} + \frac{\partial \tau_{yy}}{\partial y} + \frac{\partial \tau_{yz}}{\partial z}\right) \qquad (5)$$

$$0 = \frac{-1}{\rho}\frac{\partial \rho}{\partial z} - g \qquad P = \rho g h \qquad (6)$$

Received: 2025-10-15; Accepted: 2026-03-31
doi.org/10.62012/mp.vi.47792 | e-ISSN: 2828-6669 p-ISSN: 2828-7010

Momentum for x-direction:

$$\frac{\partial M}{\partial t}+\frac{\partial}{\partial x}\left(\frac{M^2}{D}\right)+\frac{\partial}{\partial y}\left(\frac{MN}{D}\right)+gD\frac{\partial \eta}{\partial x}+\frac{g.n^2}{D^{\frac{7}{3}}}M\sqrt{M^2+N^2}=0 \quad (7)$$

Momentum for y-direction:

$$\frac{\partial N}{\partial t}+\frac{\partial}{\partial x}\left(\frac{MN}{D}\right)+\frac{\partial}{\partial y}\left(\frac{N^2}{D}\right)+gD\frac{\partial \eta}{\partial x}+\frac{g.n^2}{D^{\frac{7}{3}}}N\sqrt{M^2+N^2}=0 \quad (8)$$

where g is gravitational acceleration, ρ is water density, P is pressure, n is Manning's roughness coefficient, and D is the total water depth. These equations govern tsunami propagation and energy transfer across the computational domain.

2.5. Shallow-Water Equations

Because tsunami wavelengths are considerably larger than the water depth, shallow-water equations provide an appropriate framework for simulating tsunami propagation [9]. These equations have been extensively applied in tsunami studies due to their computational efficiency and ability to reproduce tsunami behavior over large spatial scales [17], [18].

2.5.1. Linear Shallow-Water Equations

In deep-water environments where wave amplitudes remain relatively small compared with water depth, tsunami propagation can be approximated using linear shallow-water equations. These equations are applied in spherical coordinates to represent wave propagation over the Earth's curved surface.

$$\frac{\eta}{\partial t}+\frac{1}{R\cos\varphi}\left\{\frac{\partial P}{\partial \psi}+\frac{\partial}{\partial \varphi}(cos\varphi Q\right\}=-\frac{\partial h}{\partial t} \quad (9)$$

$$\frac{\partial P}{\partial t}+\frac{gh}{R\,cos\psi}\frac{\partial \eta}{\partial \psi}-fQ=0 \quad (10)$$

$$\frac{\partial Q}{\partial t}+\frac{gh}{R}\frac{\partial \eta}{\partial \varphi}+fP=0 \quad (11)$$

where P and Q are volume flux components, R is the Earth's radius, f is the Coriolis parameter, and ϕ and ψ denote latitude and longitude coordinates.

2.5.2. Nonlinear Shallow-Water Equations

As tsunami waves approach the coastline, decreasing water depth causes wave shoaling, resulting in increased wave amplitudes and nonlinear behavior. Therefore, nonlinear shallow-water equations are required to simulate nearshore propagation and inundation processes accurately [9]. The nonlinear shallow-water equations implemented in COMCOT are expressed in both spherical and Cartesian coordinate systems:

$$\frac{\partial \eta}{\partial t}+\frac{1}{R\,cos\varphi}\left\{\frac{\partial P}{\partial \psi}+\frac{\partial}{\partial \varphi}(\cos\varphi Q)\right\}=-\frac{\partial h}{\partial t} \quad (15)$$

$$\frac{\partial P}{\partial t}+\frac{1}{R\cos\varphi}\frac{\partial \eta}{\partial \psi}\left\{\frac{P^2}{H}\right\}+\frac{1}{R}\frac{\partial \eta}{\partial \varphi}\left\{\frac{PQ}{H}\right\}+\frac{gh}{R\cos\varphi}\frac{\partial \eta}{\partial \psi}-fQ+F_x=0 \quad (16)$$

$$\frac{\partial Q}{\partial t}+\frac{1}{R\cos\varphi}\frac{\partial \eta}{\partial \varphi}\left\{\frac{PQ}{H}\right\}+\frac{1}{R}\frac{\partial \eta}{\partial \psi}\left\{\frac{Q^2}{H}\right\}+\frac{gh}{R}\frac{\partial \eta}{\partial \psi}-fP+F_y=0 \quad (17)$$

in cartesian coordinates is formulated as follows:

$$\frac{\partial \eta}{\partial t}+\left\{\frac{\partial P}{\partial x}+\frac{\partial Q}{\partial y}\right\}=-\frac{\partial h}{\partial t} \quad (18)$$

$$\frac{\partial P}{\partial t}+\frac{\partial}{\partial x}\left\{\frac{P^2}{H}\right\}+\frac{\partial}{\partial y}\left\{\frac{PQ}{H}\right\}+gH\frac{\partial \eta}{\partial x}+F_x=0 \quad (19)$$

$$\frac{\partial Q}{\partial t}+\frac{\partial}{\partial x}\left\{\frac{PQ}{H}\right\}+\frac{\partial}{\partial y}\left\{\frac{Q^2}{H}\right\}+gH\frac{\partial \eta}{\partial y}+F_y=0 \quad (20)$$

where H represents total water depth and Fx and Fy represent bottom friction terms in the x and y directions.

2.5.3. Tsunami Simulation Model

Tsunami simulations were conducted using the Cornell Multi-grid Coupled Tsunami Model (COMCOT) developed by Wang and Power [9].

Received: 2025-10-15; Accepted: 2026-03-31
doi.org/10.62012/mp.vi.47792 | e-ISSN: 2828-6669 p-ISSN: 2828-7010

COMCOT was selected because it has been widely validated for tsunami hazard assessment and can simulate tsunami generation, propagation, and inundation using nested-grid computational techniques. The model utilized bathymetric data from BATNAS, topographic data from DEMNAS, and land-cover information derived from RBI maps. Earthquake source parameters were determined using empirical relationships proposed by Wells and Coppersmith [7], while tsunami source deformation was generated based on the specified fault geometry and focal mechanism. Three tsunami-generation scenarios were evaluated to investigate the influence of submarine landslides on tsunami characteristics. The scenarios consisted of a tectonic earthquake source combined with landslide source point 1, landslide source point 2, and a combination of both landslide sources.

3. Result

3.1. Inundation Area

Tsunami inundation in this study was analyzed using three scenarios. Scenario 1 was modeled using an earthquake fault source based on the Wells and Coppersmith formulation for Mw 6.5, combined with a landslide source at Point 1. Scenario 2 used the same earthquake fault source, combined with a landslide source at Point 2. Meanwhile, Scenario 3 combined the earthquake fault source with landslide sources at both Point 1 and Point 2. The comparison of inundation results for the three scenarios is shown in Figures 2–4.

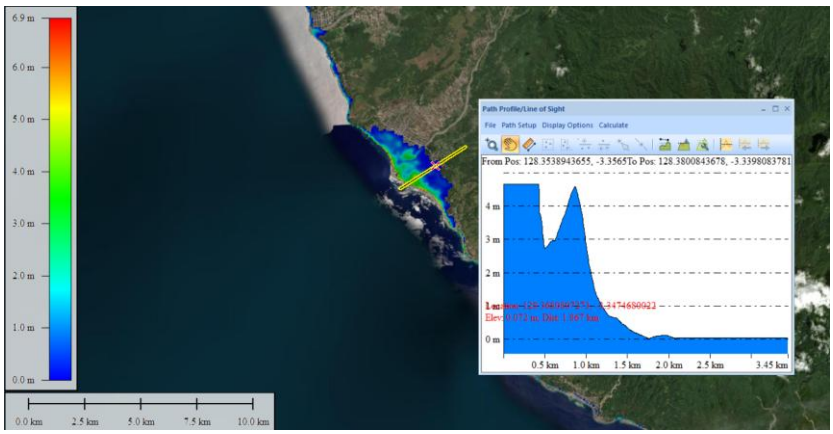

Figure 2. Scenario 1: Tsunami source based on the Wells and Coppersmith fault area for Mw 6.5 and landslide source at Point 1.

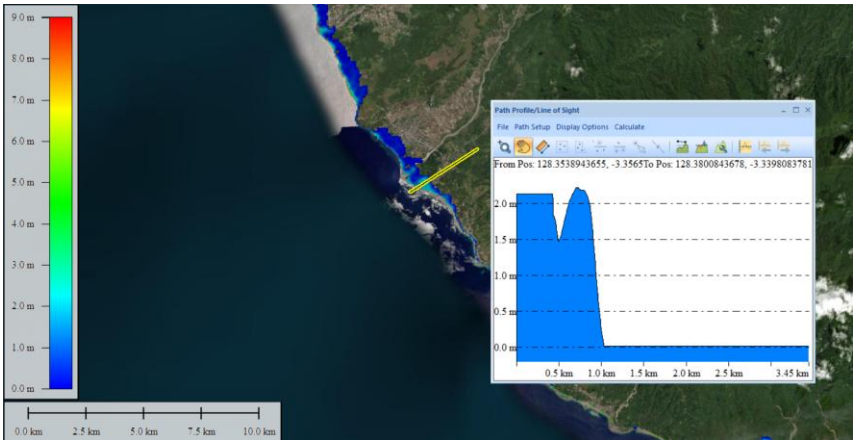

Figure 3. Scenario 2: Tsunami source based on the Wells and Coppersmith fault area for Mw 6.5 and landslide source at Point 2.

Received: 2025-10-15; Accepted: 2026-03-31
doi.org/10.62012/mp.vi.47792 | e-ISSN: 2828-6669 p-ISSN: 2828-7010

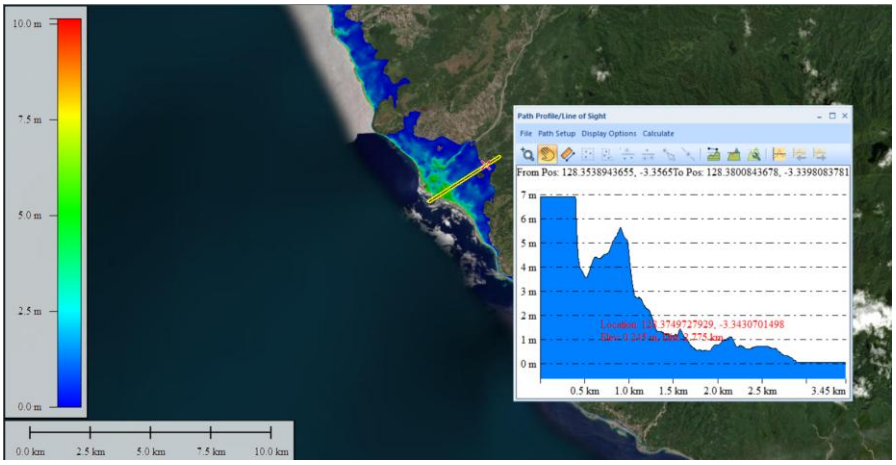

Figure 4. Scenario 3: Tsunami source based on the Wells and Coppersmith fault area for Mw 6.5 and landslide sources at Point 1 and Point 2.

The inundation results from Scenarios 1–3 indicate that 11 villages were affected by the tsunami, namely Tulehu, Waai, Liang, Kabauw, Kailolo, Pelauw, Kamarian, Pakarena, Kairatu, Waihatu, and Kamal. Based on the inundation maps, Scenario 3 produced the greatest impact compared with Scenarios 1 and 2, particularly in terms of inundation distance, inundation height, and inundation area. This is because Scenario 3 incorporated both tectonic and landslide sources at two locations, resulting in larger tsunami waves. In contrast, Scenarios 1 and 2 included only one landslide source in addition to the tectonic source.

3.2. Estimated Arrival Time and Tsunami Height

The tsunami travel time to the coastal area of Kairatu Village and its surrounding regions ranged from approximately 3 to 10 minutes at each virtual tide gauge point. The average estimated arrival time of tsunami waves along the coasts of Ambon Island and Haruku Island was approximately 4–10 minutes. The estimated time of arrival can be identified from the records of virtual tide gauges distributed across the 11 observation points, as shown in Figure 5. According to the guidelines issued by the National Tsunami Warning Centre, tsunami arrival time is determined based on the arrival of the first wave with an amplitude exceeding 50 cm.

Based on the virtual tide gauge records and tsunami propagation visualization, the first tsunami waves reached the coastal area of Kairatu Village. The waves began to arrive at Kairatu Beach in the 3rd minute. By the 5th minute, the waves had reached the coastal areas of Haruku Island, and by the 10th minute, they had reached the coast of Ambon Island.

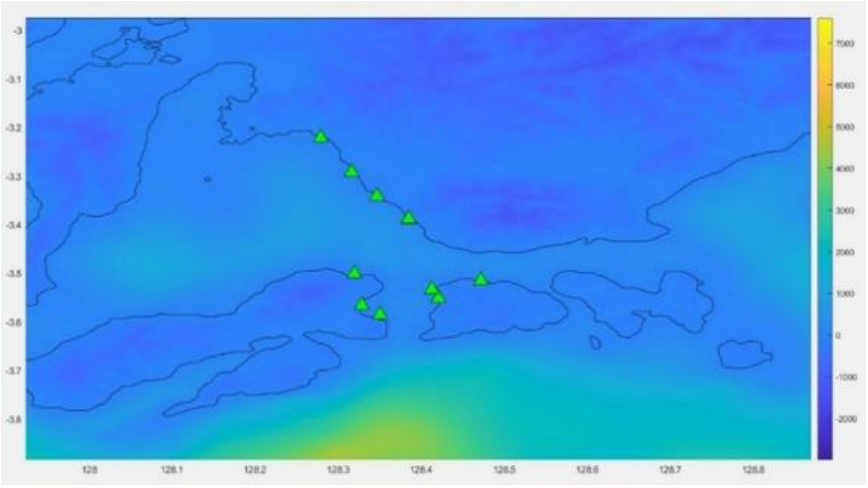

Figure 5. Locations of the virtual tide gauges.

3.5. Tsunami Hazard Potential Map

Received: 2025-10-15; Accepted: 2026-03-31
doi.org/10.62012/mp.vi.47792 | e-ISSN: 2828-6669 p-ISSN: 2828-7010

The inundation modeling results were then used to develop a tsunami hazard potential map. The tsunami hazard map was prepared based on the results of Scenario 3 because this scenario produced the most extensive and detailed inundation pattern. According to the tsunami hazard mapping guidelines issued by BNPB, a 200 m buffer zone should be applied to account for uncertainty and tolerance in the tsunami inundation boundary. The tsunami hazard potential map for the study area is presented in Figure 6.

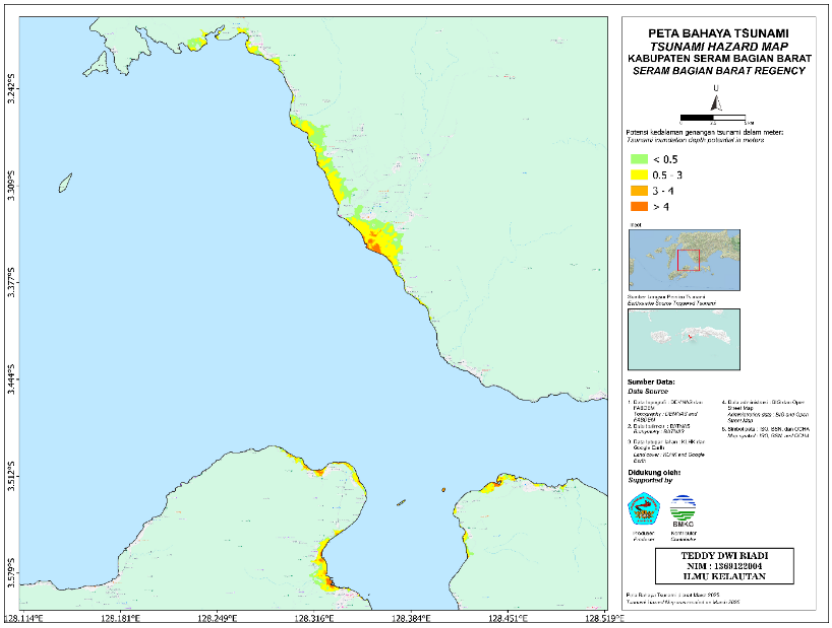

Figure 6. Tsunami hazard potential map.

Kairatu Village is the most densely populated area among the 11 affected villages in the study area. As shown in Figure 3.5, Kairatu Village has a medium to high tsunami hazard potential. This classification is based on tsunami wave height along the coastline, where an area is categorized as having high hazard potential if the tsunami wave height exceeds 3 m (BNPB, 2012). Along the Kairatu coastline, the modeled tsunami wave heights ranged from 1 to 6 m.

4. Discussion

The results of this study indicate that tsunami inundation is strongly influenced by the characteristics of the tsunami-generating sources. In this model, the tsunami was generated by a combination of tectonic earthquake sources and submarine landslide sources. Earthquake source parameters, such as magnitude, rupture dimension, displacement, and fault geometry, strongly affect the initial sea surface deformation and the subsequent tsunami propagation pattern [7], [9], [25]. In addition, submarine landslides can generate significant tsunami waves, particularly when the landslide volume, slope angle, and failure mechanism are large enough to disturb the water column [24]. The comparison among the three scenarios shows that the involvement of more than one landslide source can increase the impact of the tsunami, particularly in terms of wave height, arrival time, inundation distance, and inundated areas.

Scenario 3 produced the most extensive inundation compared with Scenarios 1 and 2. This result is reasonable because Scenario 3 included landslide sources at both Point 1 and Point 2 in addition to the earthquake source. The combination of multiple sources can increase the initial water surface displacement, which subsequently generates larger tsunami waves. As a result, tsunami waves may propagate more rapidly and reach coastal areas with greater energy. Similar tsunami numerical modeling studies have shown that variations in source parameters and bathymetric conditions can significantly influence tsunami propagation, run-up height, and flow depth distribution [17], [22], [26]. This condition explains why Scenario 3 resulted in higher tsunami hazard potential in several coastal villages, especially in areas located close to the tsunami source and low-lying coastal zones.

Received: 2025-10-15; Accepted: 2026-03-31
doi.org/10.62012/mp.vi.47792 | e-ISSN: 2828-6669 p-ISSN: 2828-7010

The modeled tsunami arrival time, which ranged from approximately 3 to 10 minutes, indicates that the study area has a very short response time for evacuation. This finding is important because communities located near the coast may have only a few minutes to move to safer areas after a tsunami is generated. Previous tsunami events in Indonesia have demonstrated that short arrival times can significantly increase disaster risk, especially in coastal settlements with limited evacuation access and preparedness capacity [11], [18], [23]. Therefore, disaster mitigation strategies in the study area should prioritize rapid evacuation planning, clear evacuation routes, early warning dissemination, and community preparedness [16], [23]. Coastal villages such as Kairatu, which showed medium to high tsunami hazard potential, require special attention due to their population density and exposure to tsunami inundation.

In addition, the inundation height and inundation extent obtained from the modeling provide important information for tsunami risk analysis. Areas with higher inundation depths and wider inundation coverage have greater potential for damage to settlements, infrastructure, public facilities, transportation facilities, and coastal economic activities. Similar hazard studies have used tsunami run-up, flow depth, and inundation extent as key parameters for assessing the level of tsunami hazard in coastal infrastructure areas [17], [20]. Therefore, the results of this study can support the development of tsunami hazard maps, spatial planning, evacuation route design, and disaster risk reduction programs in the affected villages.

However, the model results are highly dependent on the input parameters used, especially earthquake magnitude, fault characteristics, landslide volume, landslide location, slope geometry, and bathymetric conditions. If the landslide volume increases, the generated tsunami waves may become higher, and the arrival time may become shorter than the results obtained in this study. Similarly, changes in landslide thickness, width, length, and slope angle may also influence the initial wave generation and tsunami propagation pattern. Therefore, uncertainty in source parameters should be considered in future tsunami modeling studies. The use of updated seismic source maps and geological information is also important to improve the reliability of tsunami hazard assessment in Indonesia [21], [25].

The findings of this research can be used as additional reference data for tsunami hazard analysis in the study area. The key information produced in this study, including tsunami arrival time, inundation height, inundation distance, and inundation area, is essential for future risk assessment and mitigation planning. Furthermore, these results may be used as comparative data for other tsunami modeling studies, particularly those that examine the influence of combined earthquake and landslide sources on tsunami hazards in coastal regions. Numerical models such as COMCOT and other tsunami propagation models have been widely used to evaluate tsunami generation, propagation, run-up, and inundation processes, making them useful tools for comparative hazard analysis and disaster mitigation planning [13], [17], [22], [26].

5. Conclusions

Based on the tsunami modeling conducted in this study, the potential earthquake source with Mw 6.5 combined with submarine landslide sources in the Kamarian Sea and Kairatu Sea could generate tsunami waves that reach the coast of Kairatu Village within approximately 3 minutes after the tsunami is generated. The modeling results show that the tsunami wave heights varied among the three scenarios, with the highest wave occurring in Scenario 3. The maximum tsunami heights recorded in Kairatu Village were approximately 4.5 m in Scenario 1, 2.3 m in Scenario 2, and 5.8 m in Scenario 3.

The inundation mapping was carried out by processing the flow depth distribution data obtained from the tsunami model. The results indicate that the maximum inundation distance reached approximately 200 m in Kairatu Village. Among the three modeled scenarios, Scenario 3 produced the most significant impact because it involved a combination of earthquake-generated tsunami and landslide sources at both Point 1 and Point 2. This condition resulted in greater tsunami wave height, wider inundation coverage, and higher hazard potential compared with Scenarios 1 and 2.

The tsunami hazard classification in the study area, particularly in Kairatu Village, falls into the high hazard category because the modeled tsunami wave height exceeded 3 m at several

Received: 2025-10-15; Accepted: 2026-03-31
doi.org/10.62012/mp.vi.47792 | e-ISSN: 2828-6669 p-ISSN: 2828-7010

virtual tide gauge points. This classification refers to the tsunami hazard criteria established by the National Disaster Management Agency of Indonesia in BNPB Regulation No. 2 of 2012. Therefore, the results of this study indicate that Kairatu Village and surrounding coastal areas require serious attention in tsunami disaster mitigation planning, including evacuation route development, community preparedness, and coastal spatial planning.

Acknowledgments: The author expresses gratitude to Pattimura University, Meteorology, Climatology, and Geophysics Agency (BMKG) Ambon and Indonesian Geospatial Information Agency (BIG) for their support with the data and research facilities.

Data Access: https://geoportal.big.go.id/

Conflict of Interest declaration: This research has no affiliations with or involvement in any organization or entity with any financial interest in the subject matter or materials discussed in this manuscript.

References

[1] T. C. Hanks and H. Kanamori, "A moment magnitude scale," Journal of Geophysical Research, vol. 84, no. B5, pp. 2348–2350, 1979.

[2] K. Harada and F. Imamura, "Study on the effect in reducing tsunami by the coastal permeable structures," in Proceedings of the 13th Congress of the Asia and Pacific Division of the International Association for Hydraulic Engineering and Research, 2002, pp. 910–915.

[3] M. Nakamura, "Source fault model of the 1771 Yaeyama tsunami, Southern Ryukyu Islands, Japan, inferred from numerical simulation," Pure and Applied Geophysics, vol. 163, pp. 41–54, 2006.

[4] B. C. Papazachos, E. M. Scordilis, D. G. Panagiotopoulos, C. B. Papazachos, and G. F. Karakaisis, "Global relations between seismic fault parameters and moment magnitude of earthquakes," Bulletin of the Geological Society of Greece, vol. 36, 2004.

[5] D. P. Sahara, A. D. Nugraha, A. Muhari, A. A. Rusdin, S. Rosalia, A. Priyono, and E. Elly, "Source mechanism and triggered large aftershock of the Mw 6.5 Ambon, Indonesia earthquake," Tectonophysics, vol. 799, Art. no. 228709, 2021.

[6] D. Sianipar, R. Sipayung, and E. Ulfiana, "Excessive seismicity over a limited source: The August 2019 earthquake swarm near Mt. Salak in West Java, Indonesia," Journal of Seismology, vol. 24, no. 6, pp. 1189–1204, 2020.

[7] D. L. Wells and K. J. Coppersmith, "New empirical relationships among magnitude, rupture length, rupture width, rupture area, and surface displacement," Bulletin of the Seismological Society of America, vol. 84, no. 4, pp. 974–1002, 1994.

[8] M. P. Billings, Structural Geology. Englewood Cliffs, NJ, USA: Prentice Hall, 1959.

[9] L. Blaser, F. Krüger, M. Ohrnberger, and F. Scherbaum, "Scaling relations of earthquake source parameter estimates with special focus on subduction environment," Bulletin of the Seismological Society of America, vol. 100, no. 6, pp. 2914–2926, 2010.

[10] E. Bryant, Tsunami: The Underrated Hazard. Switzerland: Springer, 2014.

[11] L. Hamzah, N. T. Puspito, and F. Imamura, "Tsunami catalog and zones in Indonesia," Journal of Natural Disaster Science, vol. 22, no. 1, pp. 25–43, 2000.

[12] J. G. Hills and C. L. Mader, "Tsunami produced by the impacts of small asteroids," Annals of the New York Academy of Sciences, vol. 822, pp. 381–394, 1997.

[13] F. Imamura, A. C. Yalçiner, and G. Ozyurt, Tsunami Modelling Manual. 2006.

[14] J. Nugraha, M. Mawaleda, M. Farida, Muzli, S. Rohadi, M. Sadly, and D. K., "Pulau Seram dan sekitarnya menyimpan potensi gempabumi tektonik dalam skala besar," 2017.

[15] H. Kanamori, "Mechanism of tsunami earthquakes," Physics of the Earth and Planetary Interiors, vol. 6, no. 5, pp. 346–359, 1972.

[16] L. Kurniawan, "Perencanaan kedaruratan dalam menghadapi bencana tsunami," Alami, vol. 10, no. 2, pp. 53–57, 2005.

[17] F. A. T. Laksono, M. R. Aditama, R. Setijadi, and G. Ramadhan, "Run-up height and flow depth simulation of the 2006 South Java tsunami using COMCOT on Widarapayung Beach," IOP Conference Series: Materials Science and Engineering, Art. no. 012047, 2020.

[18] H. Latief, "Tsunami Aceh 2004," 2005. [Online]. Available: http://www.emsccsem.org/Doc/SUMATRA

Received: 2025-10-15; Accepted: 2026-03-31
doi.org/10.62012/mp.vi.47792 | e-ISSN: 2828-6669 p-ISSN: 2828-7010

_261204/Presentasi-tsunami-Aceh-hamzah.pdf. [Accessed: Dec. 20, 2022].
[19] Madrinovella, S. Widiyantoro, and I. Meilano, "Relokasi hiposenter gempa Padang 30 September 2009 menggunakan metode double difference," Jurnal Teknik Mesin, vol. XVII, no. 1, 2011.
[20] T. W. Nurhalita, "Studi tingkat bahaya tsunami terhadap bandar udara dan pelabuhan laut di Nusa Tenggara Timur," Undergraduate thesis, Program Studi Geofisika, Sekolah Tinggi Meteorologi Klimatologi dan Geofisika, Tangerang Selatan, Indonesia, 2017.
[21] Pusat Studi Gempa Nasional, Peta Sumber dan Bahaya Gempa Indonesia Tahun 2017. Bandung, Indonesia: Pusat Penelitian dan Pengembangan Perumahan dan Permukiman, Kementerian Pekerjaan Umum dan Perumahan Rakyat, 2017.
[22] P. L.-F. Liu, Y.-S. Cho, S. B. Yoon, and S. N. Seo, "Numerical simulations of the 1960 Chilean tsunami propagation and inundation at Hilo, Hawaii," in Recent Development in Tsunami Research. Dordrecht, The Netherlands: Kluwer Academic Publishers, 1994, pp. 99–115.
[23] D. Ruswandi, Indeks Risiko Bencana Indonesia Tahun 2013. Jakarta, Indonesia: Direktorat Pengurangan Risiko Bencana, Deputi Bidang Pencegahan dan Kesiapsiagaan, Badan Nasional Penanggulangan Bencana, 2014.
[24] G. Shanmugam, Slides, Slumps, Debris Flows, and Turbidity Currents. Texas, USA: Elsevier, 2013.
[25] P. M. Shearer, Introduction to Seismology. New York, NY, USA: Cambridge University Press, 2009.
[26] X. Wang and W. L. Power, COMCOT: A Tsunami Generation, Propagation and Run-Up Model. USA: GNS Science, 2011.

Received: 2025-10-15; Accepted: 2026-03-31
doi.org/10.62012/mp.vi.47792 | e-ISSN: 2828-6669 p-ISSN: 2828-7010